Maria Sklodowska-Curie Actions (MSCA)
Innovative Training Networks (ITN)
H2020-MSCA-ITN-2018
Grant number 813137

Project number 813137

URBASIS-EU
New challenges for Urban Engineering Seismology

DELIVRABLE

Work Package: WP4
Number: D4.1 – Intensity measure and engineering demand parameter for natural and induced seismicity.

Authors:	**Ghimire, Subash**	(UGA)
Co-Authors:	Gueguen, Philippe	(UGA)
	Schorlemmer Danijel	(GFZ)

Reviewers	Astorga, Ariana
Approval	Management Board
Status	Final Version
Dissemination level	Public
Delivery deadline	31.10.2020
Submission date	18.02.2021
Intranet path	https://urbasis-eu.osug.fr/Scientific-Reports-157

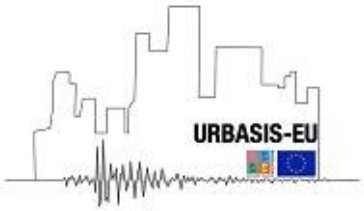

Abstract

Performance-based earthquake engineering is a probabilistic decision-making framework aimed to mitigate seismic risk, based on a comprehensive scientific foundation. In this framework, the ground motion intensity measures (IM) is linked to the threshold damage parameters (EDP) to measure the expected damage of the structures. Two natures of IM are defined: (1) an efficient IM defined as providing the smallest variability in EDP given IM relation, and (2) sufficient IM defined as providing EDP conditionally independent on earthquake magnitude and distance. Most of the studies use numerical methods to model the building response for given IM. Experimental data from the full-scale observations are much more representative of the complex physical process than even the most sophisticated laboratory or numerical experiments. Integrating these data into our modes helps to identify the sources of epistemic uncertainty. The objective of this study is to use experimental data collected from the buildings to explore the sources of epistemic uncertainties in EDP given IM relationship (i.e. $\sigma_{EDP|IM}$) and to test the IM efficiency and sufficiency. For this, we developed a database by collecting real strong motion values recorded at the top and at the bottom floors of the buildings from the US, Japan, and Romania. The database contains 8,520 strong motion recordings that correspond to 118 buildings and 2,737 events. Several ordinary and spectral IMs are considered as ground motion IM and the normalized relative roof displacement of the building is considered as EDP. The relationship between EDP given IM is analyzed in order to identify the associated sources of uncertainties (i.e. $\sigma_{EDP|IM}$). Region-to-region, building-to-building, and within-building uncertainties associated with earthquake magnitude-distance and aging is explored. The efficiency and sufficiency of each IM from a large set of building and earthquake motion data are tested for different criteria characterizing the seismic source (magnitude and source-to-site distance) and considering several building classes, and a specific single-building analysis including aging due to cumulative earthquake damage over time. Empirical building damage prediction equation is developed by utilizing the available experimental data and considering the most efficient IMs.

1. Introduction

The performance-based earthquake engineering (PBEE) framework is developed by the Pacific Earthquake Engineering Research to assist decision-makers in seismic risk decision making. PBEE is based on a comprehensive response analysis of an individual component in a probabilistic framework (Porter, 2003). PBEE framework is divided into four stages: hazard analysis, structural response analysis, damage analysis, and consequences analysis. In hazard analysis, the ground shaking potential is defined in terms of ground motion intensity measures (IM) and their annual frequency of exceedance (λ_{IM}) through probabilistic seismic hazard assessment. In structural analysis, the response of the structure to a given IM is expressed in terms of engineering demand parameters (EDPs), such as structural drift, maximal top acceleration, etc. In damage analysis, damage measurement (DM) is calculated based on threshold of EDP values and models of structure capacity or fragility. Finally, the earthquake's consequence is measured in terms of repair costs, the operability of the structure, and potential economic or human losses for a given DM. The consequences can be expressed as decision variables (DVs) on which decision-makers can base their decisions in view of the expected performance levels. The four steps of the underlying probabilistic framework of PBEE estimate the frequency of failure of a performance level over a given period of time; this involves uncertainties. For example, the annual frequency of exceeding a given EDP value (λ_{EDP}) is expressed by:

$$\lambda_{EDP} = \int_{im} P[EDP/IM = im]|d\lambda_{im} \quad (1)$$

where P(EDP|IM=im) is the conditional probability of occurrence of each EDP value, taking into account the value of the IM, and $d\lambda_{im}$ is the annual rate of exceeding an IM value, derived from the hazard curves. P(EDP|IM=im) is usually obtained by considering a series of nonlinear dynamic analyses of the structure.

Baker and Cornell (2008) provide a detailed description of approaches to characterize and propagate uncertainties at each step. Current research on PBEE is mainly focused on identifying the origins of uncertainties, distinguishing between epistemic and random uncertainties, in order to boost scientific efforts on the reducible elements that contribute most to the performance uncertainty (Iervolino, 2017). In practice, P(EDP|IM=im) satisfies a chosen model of EDP distribution for a given IM and is obtained by regression of EDP values for IM values. Baker and Cornell (2008b), Luco (2002), and Luco & Cornell (2007) defined two natures of IM: efficient and sufficient. IM that results in the smallest degree of variability around the regression of EDP on the IM values is defined as an efficient IM. Similarly, IM that results EDP values conditionally independent on earthquake magnitude and epicentral distance is defined as sufficient IM. Structure response and the associated uncertainties are conditioned by time-history seismic excitation, considering the IM at which the EDP value is exceeded. Several authors investigated the efficiency and sufficiency of IM (e.g. Baker & Cornell, 2008b; Bianchini et al., 2009; Buratti, 2012; Eads et al., 2015; Ebrahimian et al., 2015; Jayaram et al., 2011; Luco, 2002; Luco et al., 2005; Luco & Cornell, 2007; Mollaioli et al., 2011; Vamvatsikos & Cornell, 2005). All these studies are based on the numerical modeling of structures considering different ground motion datasets, mostly using the Incremental Dynamic Analysis approach (IDA). Structural analysis through numerical approach involves the selection or generation of natural or synthetic accelerograms from different tectonic areas, the scaling applied to obtain the desired structural response values, the selection of physical modal parameters (e.g., structural period and damping) and their co-seismic variations, as well as other modeling assumptions related to component fragility functions, affect the overall uncertainty of the performance estimate. Furthermore, a typical assumption in the assessment of P(EDP|IM) is that the building response variability for a class of buildings is the same as the response variability for a given building in this class (this assumption is an ergodic assumption affecting fragility curves).

According to several authors (e.g. Guéguen et al., 2016, Trifunac et al., 2010), studies carried out by considering the data from full-scale observations in real buildings are much more representative of the complex structural response than even the most sophisticated laboratory or numerical experiments; one way of improving engineering science to understand the physical behavior of structures is to use a complete database of earthquake recordings in real structures. For example, Perrault and Guéguen (2015) analyzed the variability of EDP versus IM using accelerometric data recorded in Californian buildings, taking structural drift as the EDP, and developed building damage prediction equation (BDPE) with its associated uncertainties. Astorga et al. (2018, 2019, 2020) completed the analysis, confirming the added value of physical data in understanding the

seismic response of Japanese buildings in terms of co-seismic demand parameters related to modal (i.e. resonance frequency) parameter variations, especially during repetitive earthquake sequences.
In this study, the efficiency and sufficiency of several IMs for P(EDP|IM) from a large number of experimental datasets are analyzed by using the regression model of EDP values for IM values. In the second section, a database developed by collecting earthquake and building response parameters is described. The third section describes the method used to explore the uncertainty in EDP|IM relation. Then, the results in terms of efficiency and sufficiency are discussed in the fourth section, completed in the fifth by a specific analysis on the variation of the co-seismic frequency value versus EDP. Finally, the conclusion develops a simple empirical BDPE using available experimental data and the most efficient IMs.

2. Description of the database

A database is developed by collecting accelerometric data recorded in buildings from the strong motion networks from the US, Japan, and Romania. For each earthquake, information such as magnitude and epicentral distance is available but there is no description of the source parameters. Similarly, for each building, information such as geographic location, height, material, number of floors, etc. are available. From the accelerometric recordings ground motion intensity measures and building response parameters are computed for each earthquake. Ground motion IMs and the buildings response parameters were computed along the two direction of the buildings. The detail description of the database is available in Astorga et al (2020). Below sections present the information that are included in the database:

2.1 Building and earthquake characteristics

For each building the name of the strong motion network monitoring the building, building's identification, geographic location, height, number of floors, and the soil properties at building location are collected (Tab. 1). Similarly, the event identification, geographic location, magnitude, and epicentral distance are also collected for each earthquake (Tab. 2).

Table 1. Building's information included in the database.

ID	Description	Units
Network ID	Strong motion network operator.	
Building ID	Building identification code, subscript x and y represents the two orthogonal direction.	
B-Latitude	Geographic latitude of the building.	degree
B-Longitude	Geographic longitude of the building.	degree
Vs_{30}	Average shear wave velocity of the site at a depth of between 0 and 30 meters.	m/s
Height	Distance between the top and bottom sensors.	cm
Floors	Total numbers of floors in the building.	
Materials	Structural material used in the building.	

Table 2. Earthquake's information included in the database.

Event ID	Name of the record containing the building and earthquake information.	
E-latitude	Latitude of the epicenter.	degree
E-longitude	Longitude of the epicenter.	degree
Magnitude	Magnitude of the earthquake.	M_w or M_{JMA}
Epicentral distance	Distance of the epicenter from the building.	km

2.2 Building response parameters

Six building response parameters are computed using the accelerometric data recorded at the top floor of each building. These parameters are: pre- and co-seismic fundamental frequency, peak top acceleration (PTA), velocity (PTV), displacement (PTD), and the drift ratio (Tab. 3).

Table 3. Building response parameters included in the database.

ID	Description	Units
f_i	Elastic frequency, i.e. pre-seismic fundamental frequency.	Hz
f_{min}	Minimum value of the fundamental frequency during the earthquake, co-seismic fundamental frequency.	Hz
PTA	Peak acceleration recorded at the building's top floor sensors.	cm/s^2
PTV	Peak velocity computed at the building's top floor sensors.	cm/s
PTD	Peak displacement computed at the building's top floor sensors.	cm
Drift ratio	Maximum relative displacement between the top and bottom sensors normalized by the height of the building.	cm/cm

The f_i corresponds to the elastic fundamental frequency, computed by the Fourier transform of the zero-padded (16,384samples) prevent noise window. Similarly, the f_{min} corresponds to the co-seismic minimum value of the fundamental frequency computed from the time-frequency distribution of each record. Astorga et al. (2018) explained the detail procedure to compute f_i and f_{min}. The co-seismic time-frequency variation is associated to structural health and nonlinear processes involved in the building during loading (e.g. Todorovska & Trifunac, 2007; Astorga et al. 2018, 2019).

2.3 Ground motion intensity measures

Ground motion IMs values are computed from the accelerometric data recorded at the bottom floor of each building. Six ordinary intensity measures are considered, these ground motion IMs are: Peak ground acceleration (PGA), velocity (PGV), and displacement (PGD), arias intensity (AI), destructive potential (DP), and cumulative absolute velocity (CAV) (Tab.4). The PGA, PGV, and PGD corresponding to the absolute values of maximum acceleration, velocity, and displacement time histories, respectively. Arias intensity (Arias, 1970) includes both the amplitude and duration of seismic shaking, computed as follows:

$$AI = \frac{\pi}{2g}\int_0^{tf} a^2(t)dt \quad (2)$$

where g is the acceleration due to gravity, $a(t)$ is the acceleration recorded at time t, and t_f is the total duration of the recording. Cumulative absolute velocity (EPRI, 1988) is computed as follows:

$$CAV = \int_0^{tf} |a(t)|dt \quad (3)$$

where |a(t)| is the absolute value of acceleration at time t. Finally, destructive potential (Araya & Saragoni, 1984) is a modification of AI, taking into account the frequency content of the ground motion. DP is defined as follows:

$$DP = \frac{AI}{{v_0}^2} \quad (4)$$

where ${v_0}^2$ is the number of zero crossings per time unit.

Similarly, six spectral IM values are considered, these spectral intensity measures are: spectral acceleration (5% damping) (SA1 and SA2), velocity (SV1 and SV2), and displacement (SD1 and SD2) for two specific frequency values (1 and 2) impacting seismic demand (Tab. 4). Index 1 corresponds to the spectral value computed at the elastic frequency of the system f_i and index 2 corresponds to the minimal co-seismic value of the resonance frequency f_{min}.

In addition, three mean spectral values are computed between f_{min} and f_i (Avg_Sa, Avg_Sv, and Avg_Sd) (Tab. 4). These average response spectral values take into account the frequency shift that occurs during the seismic loading, and co-seismic non-linear response of the building (Perrault and Guéguen, 2015).

Table 4. Ground motion intensity measures included in the database.

ID	Description	Units
PGA	Peak ground acceleration recorded by the bottom sensor of the building.	cm/s^2

PGV	Peak ground velocity computed at the bottom sensor of the building.	cm/s
PGD	Peak ground displacement computed at the bottom sensor of the building.	cm
AI	Arias intensity.	cm/s
DP	Destructive potential.	cm*s
CAV	Cumulative absolute velocity.	cm/s
SA1	Pseudo-spectral acceleration for the spectral frequency of f_i (5% damping).	cm/s^2
SV1	Pseudo-spectral velocity for the spectral frequency of f_i (5% damping).	cm/s
SD1	Pseudo-spectral displacement for the spectral frequency of f_i (5% damping).	cm
SA2	Pseudo-spectral acceleration for the spectral frequency of f_{min} (5% damping).	cm/s^2
SV2	Pseudo-spectral velocity for the spectral frequency of f_{min} (5% damping).	cm/s
SD2	Pseudo-spectral displacement for the spectral frequency of f_{min} (5% damping).	cm
Avg-Sa	Mean pseudo-spectral acceleration between f_i and f_{min} (5% damping).	cm/s^2
Avg-Sv	Mean pseudo-spectral velocity between f_i and f_{min} (5% damping).	cm/s
Avg-Sd	Mean spectral displacement between f_i and f_{min} (5% damping).	cm

2.4 Strong motion duration parameters

Sixteen strong motion duration parameters are computed from the accelerometric time-histories data recorded at the bottom floor of each building (Tab. 5). Strong motion duration parameters were computed along the two different directions of the buildings. The strong motion duration considered are:

- Bracketed duration, D_B (Fig. 1a): the total time between the first and the last exceedance of a specific acceleration threshold (i.e. a_0). Four acceleration thresholds are defined: 0.05g (i.e. D_{B1}), 0.1g (i.e. D_{B2}), 0.15g (D_{B3}), and 0.20g (D_{B4}).
- Effective duration, D_E (Fig. 1b): defined by $D_E = t_f - t_0$, where t_0 corresponds to the time at which 0.01m/s of cumulative energy is reached in the Husid diagram (i.e. energy build-up plot, AI) and t_f corresponds to the time at which AI=0.125 m/s
- Uniform duration, D_U: the sum of the time intervals during which acceleration exceeds a specific acceleration threshold. Four acceleration thresholds are considered: 0.05g (i.e. D_{U1}), 0.1g (i.e. D_{U2}), 0.15g (i.e. D_{U3}), and 0.20g (i.e. D_{U4}).
- Significant duration, D_S (Fig. 1b): defined as the time interval over which a specific percentage of total energy is accumulated on the Husid diagram. Intervals corresponding to (5-75)% and (5-95)% of total energy computed from acceleration are considered, indicated as D_{Sa1} and D_{Sa2}, respectively. Similarly, durations based on cumulative energy computed from velocity (i.e. D_{Sv1} and D_{Sv2}) and displacement signals (i.e. D_{Sd1} and D_{Sd2}) are also computed, as suggested by Trifunac and Brady (1975).
- Zhou and Xie (1984) duration, D_{ZX}, defined as:

$$D_{ZX} = \sqrt[2]{\frac{\int_0^{t_r}(t-t_c)^2 a^2(t)dt}{\int_0^{t_r} a^2(t)dt}} \; ; \; tc = \frac{\int_0^{t_r} t.a^2(t)dt}{\int_0^{t_r} a^2(t)dt} \quad (5)$$

where t_c is the center of gravity of $a^2(t)$ along the time axis, a(t) is the acceleration at a given time t, and t_r is the total duration of ground motion.

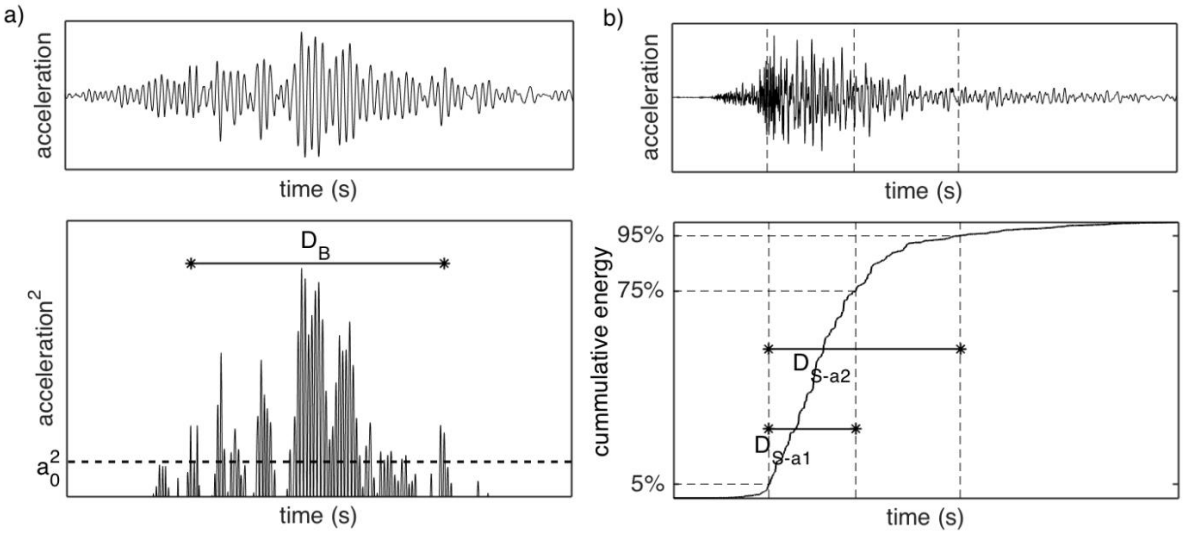

Figure 1. Schematic view of several duration definitions given for two different acceleration time histories. (a) Bracketed duration. The horizontal dashed line corresponds to the threshold level of acceleration. (b) Significant strong motion duration computed for (5-75) % and (5-95) % of total energy based on the Husid diagram.

Table 5. Strong motion duration parameters included in the database.

ID	Description	Units
D_E	Time interval between 0.01m/s and AI=0.125 m/s using the Husid diagram.	s
$D_{B\ (1,2,3\ or\ 4)}$	Total time between the first and the last exceedance of the acceleration threshold, i.e. 0.05g (D_{B1}), 0.10g (D_{B2}), 0.15g (D_{B3}) and 0.20g (D_{B4}).	s
$D_{U\ (1,2,3\ or\ 4)}$	Sum of the time intervals during which acceleration exceeds the acceleration threshold, i.e. 0.05g (D_{U1}), 0.10g (D_{U2}), 0.15g (D_{U3}) and 0.20g (D_{U4}).	s
$D_{Sa\ (1or\ 2)}$	Duration corresponding to (5-75) % (i.e. D_{Sa1}) and (5-95) % (i.e. D_{Sa2}) of total energy associated with ground motion acceleration.	s
$D_{Sv\ (1or\ 2)}$	Duration corresponding to (5-75) % (i.e. D_{Sv1}) and (5-95) % (i.e. D_{Sv2}) of total energy associated with ground motion velocity.	s
$D_{Sd\ (1or\ 2)}$	Duration corresponding to (5-75) % (i.e. D_{Sd1}) and (5-95) % (i.e. D_{Sd2}) of total energy associated with ground motion displacement.	s
D_{ZX}	Zhou and Xie (1984) duration.	s

2.5 Building earthquake early warning parameters

Earthquake early-warning system is designed to disseminate the information about earthquake once detected by the earthquake early warning system. The building earthquake early-warning parameters facilitates to predict the potential building response during the earthquake. We compute three building earthquake-early waring parameters by using the accelerometric time-histories recorded at the top and bottom floor of the building along two direction of the building. These building early parameters are: peak value of the displacement, integral of the square of the velocity, and the displacement (Tab. 6). They are computed in the first three seconds of the p-wave window.

$$Pd = \max_{t_p \le t \le t_p+\tau} |d(t)| \quad (6)$$

$$IV^2 = \int_{t_p}^{t_p+\tau} v^2(t)\, dt \quad (7)$$

$$ID^2 = \int_{t_p}^{t_p+\tau} d^2(t)\, dt \quad (8)$$

where t_p is the first arrival time, τ is the window length and $d(t)$ is the displacement and $v(t)$ is the velocity.

Table 6. Building earthquake early warning parameters included in the database.

ID	Description	Units
Pd	Peak of the displacement	cm
IV^2	Integral of the squared of the velocity	cm^2/s
ID^2	Integral of the squared of the displacement	$cm^2.s$

2.6 Dataset

Fig. 2 (a) shows the geo-localization of the buildings and the earthquakes and (b) distribution of earthquake magnitude and epicentral distance, and (c) distribution of peak of ground acceleration available in the database. The description of the datasets present in our database is given below:

US data - Data from 84 US buildings provided by Center for Engineering Strong Motion Data (CESMD) (https://strongmotioncenter.org/) were considered. The distribution of the buildings according to construction material is as follows: 27% reinforced concrete (US-RC), 57% steel (US-ST), 11% masonry (US-MA), and 5% wood (US-WO). 684 accelerometric recordings were collected; among them, 225/302/134/24 recordings were collected from concrete/steel/masonry/wooden buildings, respectively. Moment magnitude (M_w) varies from 3.5 to 7.3 and epicentral distance varies from 2.6 to 331 km (Fig. 2b). The dataset includes strong earthquakes, such as the 7.2 M_w Landers event in 1992 and the 7.3 M_w Baja California event in 2010. Two subsets of Californian data are considered to assess uncertainties related to the tectonic context. These subsets are named specific tectonic source STS1 and STS2. The latitude and longitude boundaries of STS1 and STS2 are 33 to 35 and 35 to 39 degrees; 116 to 120 and 120 to 123 degrees, respectively (Fig. 2a).

RO data - A ten-story reinforced concrete building monitored by the National Center for Seismic Risk Reduction (NCSRR) of Romania is considered. This building has been monitored since December 2013. 108 accelerometric records were collected, most of them corresponding to earthquakes located in the Vrancea seismic zone to the north of Bucharest (Fig. 2a). Epicentral distance thus varies slightly, between 127 and 178.3 km for M_w ranging from 3.8 to 5.6 (Fig. 2b). The largest earthquakes M_w 5.6 and 5.4 in 2016 and 2014, respectively, are included.

JPN data – 11,763 accelerometric recordings from 32 high/mid-rise Japanese buildings were collected from the BRI strong motion network (https://smo.kenken.go.jp/) (Fig. 2a). The building distribution according to elementary typology is as follows: 24% steel (JPN-ST), 40% reinforced concrete (JPN-RC), and 36% steel-reinforced concrete (JPN-SRC). The main shock and aftershock sequences of the strongest earthquake, 2011 Tohuku, are included. Magnitude varies from 2.6 to 9.1 (JMA magnitude) and epicentral distance varies from 2.2 to 2,394 km (Fig. 2b).

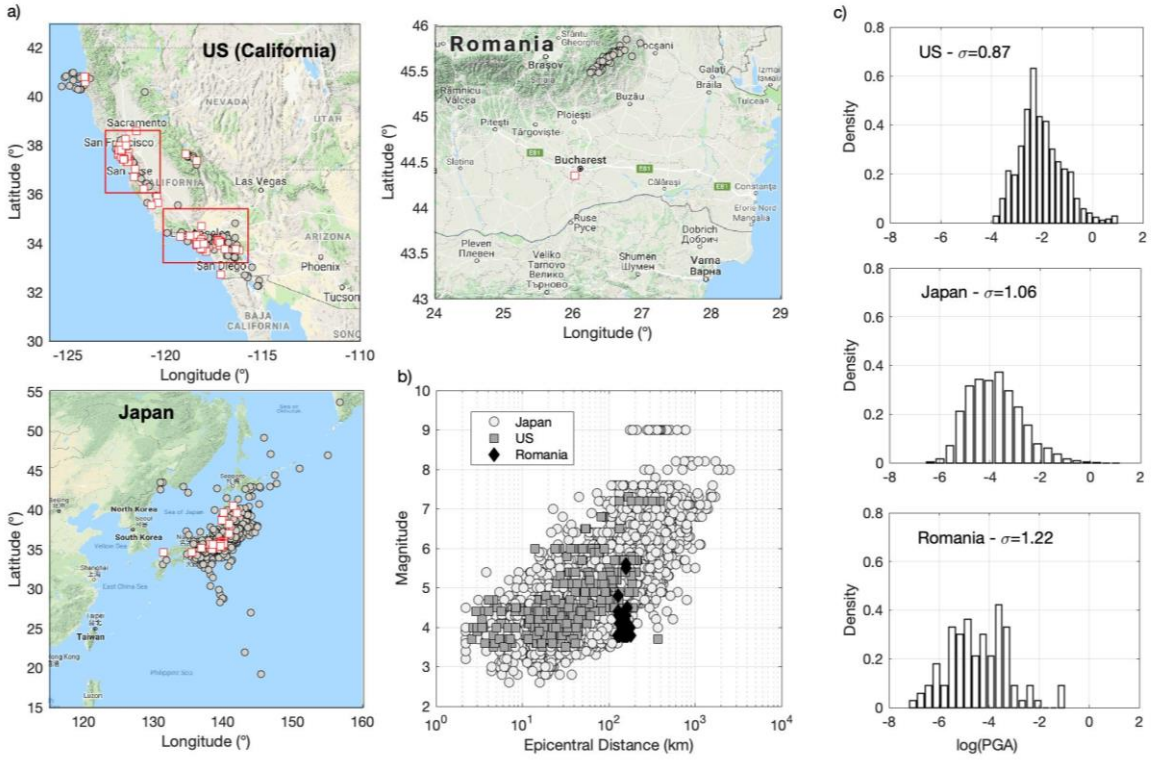

Figure 2. View of the whole dataset used in this study. (a) Positions of epicenters (gray circles) and buildings (red squares) in the US (California), Romania and Japan. For the US dataset, the two red rectangular boxes define the area of the two specific regions discussed in the manuscript. (b) Magnitude versus epicentral distance distribution of the whole dataset including Japan (open circles), the US (gray squares) and Romania (solid diamonds). (c) Distribution of natural log(PGA) for American, Japanese and Romanian datasets, respectively. σ is the standard deviation of the distribution.

ANX – One of the Japanese buildings, ANX, is a building that has been studied extensively by the BRI strong motion network. A detailed description of ANX is available in Astorga et al. (2018). ANX is an 8-story, steel-reinforced concrete building located approximately 60km northwest of Tokyo, in Tsukuba (Japan) (Fig. 3a). ANX has one basement floor resting on spread foundations (8.2 m deep) lying on soft soil made up of alternating layers of clay and sandy-clay to a depth of 40 m. A description of the instrumentation is provided by Kashima (2004, 2014). The ANX dataset is the largest of our datasets, comprising 1,630 recordings in both horizontal directions, made over a period of 20 years, starting immediately after building completion in March 1998 and including the main shock and aftershocks of the 2011 Tohuku earthquake. Magnitude varies from 2.6 to 9.1 and epicentral distance varies from 2.2 to 1,730 km. (Fig. 3b). Furthermore, three data subsets are defined using ANX dataset based on the distribution of magnitude-distance criteria is considered to have an adequate number of data in each dataset (Fig. 3b): MR1 corresponding to 166 entries with R = 20 ± 50% and M= 3.5 ± 0.5; MR2 corresponding to 575 entries with R =120 ± 60% and M= 4.5 ± 0.5 and MR3 corresponding to 274 entries with R = 250 ± 70% and M= 5.5 ± 0.5). The distribution of peak ground acceleration for MR1/MR2/MR3 is shown in Fig. 3(c). Astorga et al. (2018, 2019) analyzed the time variation of the resonance frequency of the ANX building since 1998. They defined four time periods corresponding to changes in its behavior. During the first period (T1), the fundamental frequency starts to decrease immediately after the completion of construction work, from 1998 to 2005. Frequency stabilizes during period T2 (2006-2011/02/30) until the Tohoku earthquake sequence in 2011. During period T3, the fundamental frequency drops significantly and a slow recovery of the resonance frequency is observed directly after the Tohoku earthquake during the immediate aftershock sequence between 2011/03/01 and 2011/09/30. Finally, T4 corresponds to the period between 2011/10/01 and 2018/05/15. T1/T2/T3/T4 comprise a total of 366/313/402/468 data, respectively. Four further subsets of data within the magnitude distance criteria MR2 are considered according to

the period criteria: T1-MR2 (118 data), T2-MR2 (119 data), T3-MR2 (193 data), and T4-MR2 (121 data).

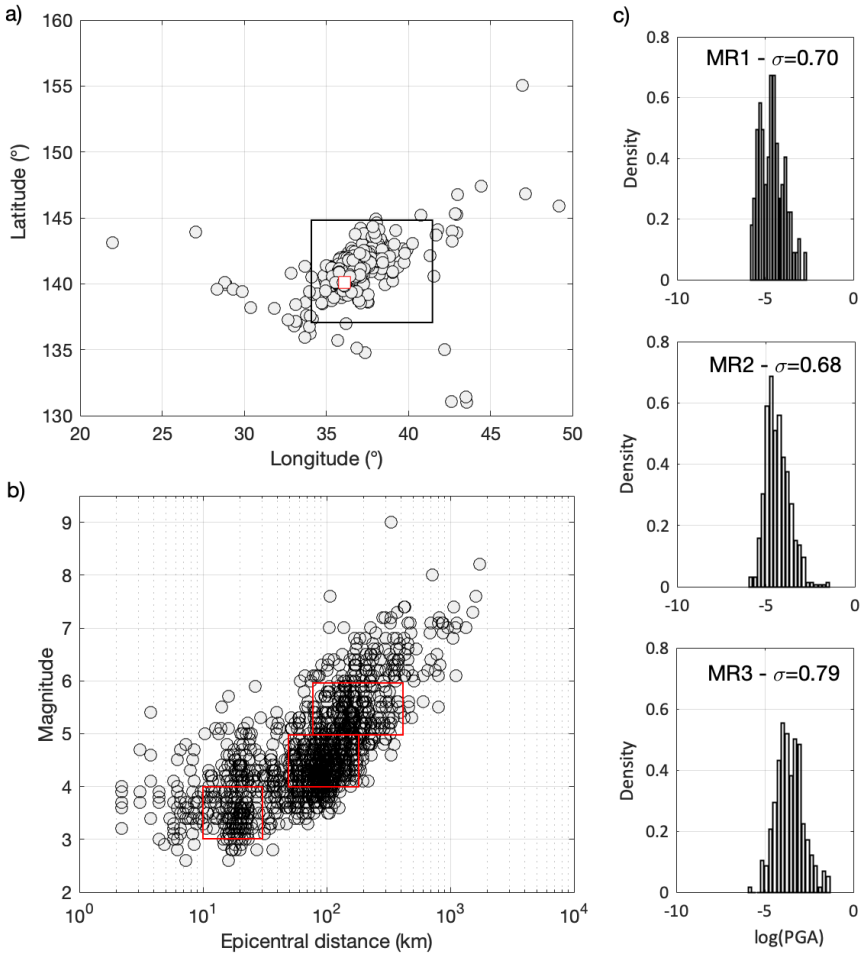

Figure 3. Dataset for the specific Annex (ANX) building in Japan. (a) Location of the ANX building (red square) and related earthquake epicenters (gray circles). The black square represents the specific subset of data considered. (b) Magnitude versus epicentral distance distribution. The red rectangles define the boundaries of the three magnitude-distance criteria (MR1, MR2 and MR3) described herein. (c) Distribution of log(PGA) for specific magnitude-distance criteria MR1, MR2 and MR3. σ is the standard deviation of the distribution.

3. Method

In this study, to explore the building response prediction uncertainties and efficiency and sufficiency of IM the drift ratio is considered as EDP and PGA, PGV, PGD, AI, DP, CAV, SA1, SA2, SV1, SV2, SD1, and SD2 are considered as IMs. IMs and EDP values corresponding to the longitudinal direction of the building is analyzed. One parameter log-log regression model (Eq. 9) of EDP on IM proposed by Luco (2002) is used to analyze the variation of variability. The degree of scattering around the fitted model represents the uncertainty of the EDP|IM model i.e. $\sigma_{EDP|IM}$.

$$log(EDP) = a + b.log(IM) + \varepsilon \quad (9)$$

where a and b are the estimated regression coefficients and ε is the standard error.

The variability associated with IMs and EDP is represented hereafter as σ_{IM}, and σ_{EDP}, respectively, i.e. the standard deviation of the log of IM and EDP values, normalized by their mean value.

The efficiency and sufficiency of IMs is also tested. The efficiency of IMs is defined simply as the IM that results in a small variability of EDP given IM value i.e. $\sigma_{EDP|IM}$. The sufficiency of IMs is defined as the IM that makes EDP conditionally independent on earthquake parameters such as magnitude (M) and source-to-site distance (R). Sufficiency is tested by computing the linear regression between EDP and IM regression residuals ((ε|IM) of Eq.9 and the corresponding

value of M or log(R) (Luco & Cornell, 2007). The statistical significance of the coefficient obtained from the standard linear regression for M and log(R) is assessed based on the p-value (i.e. the probability of obtaining an estimated value of the coefficient at least as large as the actual value, the actual value of the coefficient being zero) (Benjamin & Cornell, 1970). If the p-value observed is greater than or equal to 0.05, the estimated coefficient of M or log(R) is statistically insignificant and the IM is considered sufficient (Luco & Cornell, 2007).
Fig. 4 shows the distribution of residual values EDP|PGA for the whole dataset, versus M or log(R). As expected, $\sigma_{EDP|PGA}$ varies significantly, reflecting several sources of uncertainties, which will be explored in the following section.

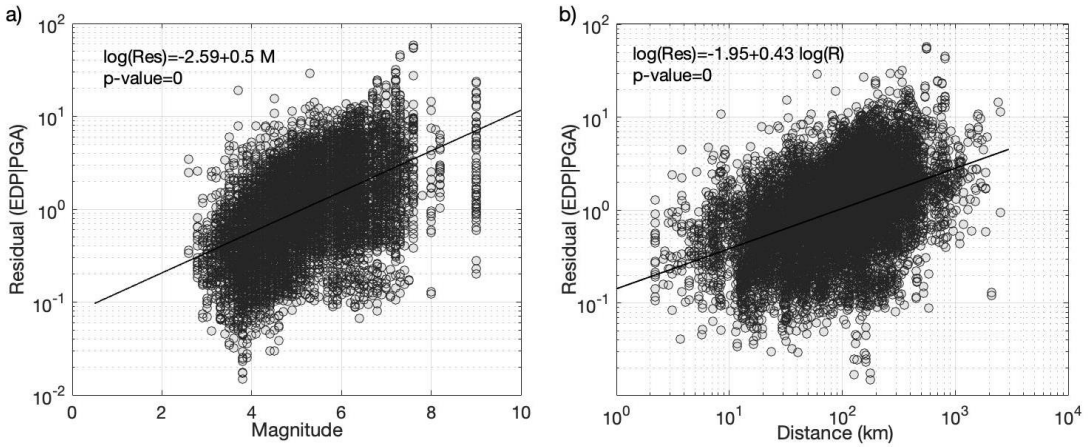

Figure 4. Distribution of residual values (EDP|PGA) as function of (a) M and (b) log(R), considering the whole dataset. The lines represent the fitted linear model between log(R)/M and the residuals.

4. Result on building response prediction uncertainties

4.1 General trends - σ

Fig. 5 shows the standard deviation of the residuals of the fitted standard log-linear regression model between EDP and IM (Eq.6) for ALL (JPN+US+RO) datasets. For each IM parameter, σ_{IM} is given in Fig. 5b. All the σ_{EDP}, σ_{IM}, and $\sigma_{EDP|IM}$ values are provided in Appendix A1.
The first observation is that the JPN dataset (σ_{EDP}=1.44), largest in terms of numbers, is predominant in our global dataset (1.48) compared with the US dataset (1.32). $\sigma_{EDP|IM}$ variability (Fig. 5a) oscillates between 0.8 and 1.1, with the highest values corresponding to the spectral and ordinary acceleration values and DP intensity measures. However, for AI and DP, it is important to note that $\sigma_{EDP|IM}$ remains similar to the other values, while the associated IM σ_{IM} varies considerably. This indicates that these parameters are not good indicators of the natural variability of ground motion and do not enable a high degree of certainty for predicting the response of structures. The most efficient IMs are in velocity (i.e. PGV, SV1, and SV2), with $\sigma_{EDP|IM}$ corresponding to 0.80, 0.79 and 0.79, respectively. The efficiency of these velocity IMs has already been reported for US data by Perrault and Guéguen (2015) and is confirmed herein, regardless of the dataset considered.
In order to capture the origins of the uncertainties in building response prediction, several relationships are tested in the following sections, according to tectonic region, building typology, and ageing effect. The paucity of the data for specific analysis in some datasets makes it necessary to separate the studies; sub-datasets are therefore presented.

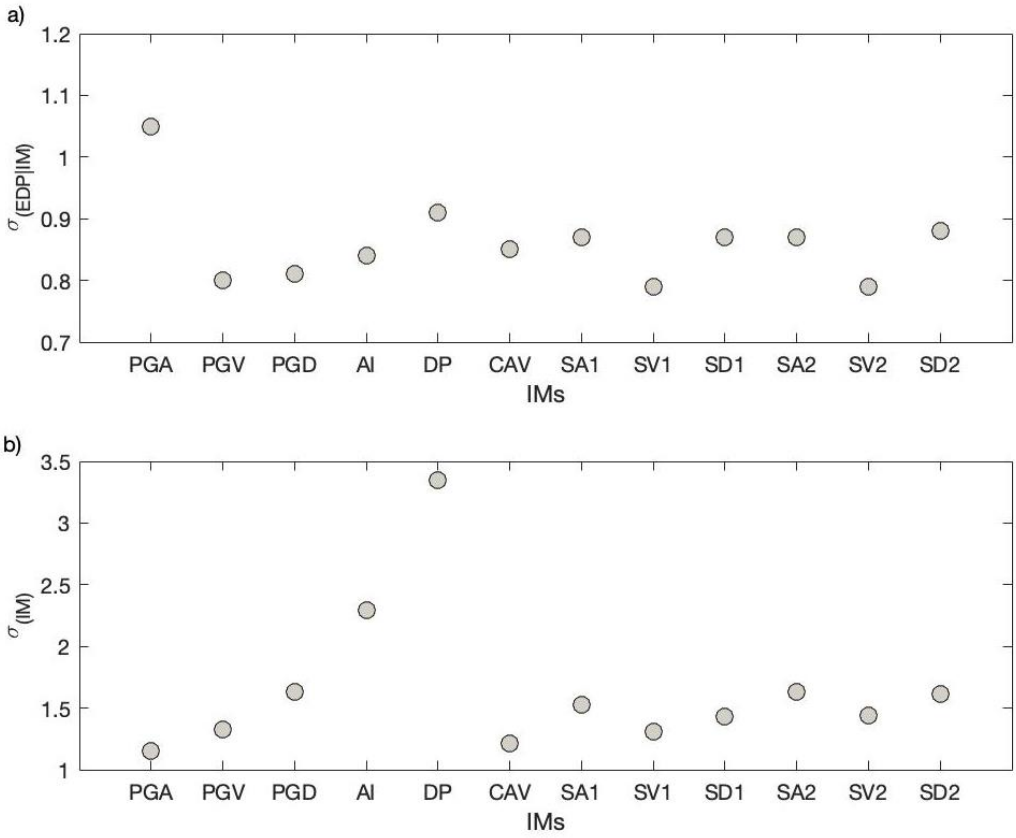

Figure 5. (a) $\sigma_{EDP|IM}$ values for the IMs concerned, computed for the whole dataset. (b) σ_{IM} values.

4.2 Variability associated with the tectonic context - σ_R

In this study, the effect of tectonic region on building response is explored using the STS1 and STS2 dataset (Fig.2) considering all building typologies from the US dataset. Note that for STS1 and STS2, the σ_{EDP} values are the same (1.24 and 1.20 respectively, Appendix A1), and σ_{IM} differs only marginally. In Fig. 6, the effect of considering the data by specific region barely minimizes the $\sigma_{EDP|IM}$ values, for the same values of σ_{IM} (Fig. 6b). The figure shows that for velocity IMs (i.e. PGV, SV1 and SV2), the $\sigma_{EDP|IM}$ values are similar, being around 1 for ALL, STS1 and STS2 (values in Appendix A1). On the other hand, the $\sigma_{EDP|IM}$ values for STS1 and STS2, respectively, correspond to 1.15 and 0.97 for SA1, 1.15 and 1.04 for SA2, 1.03 and 1.10 for SD1 and 1.03 and 1.10 for SD2. Thus, a trend inversion (the smallest values for STS2 or STS1) is observed depending on whether acceleration or displacement IM values are considered. Although the origin of this inversion has not been confirmed, the class of the buildings concerned in these two geographical areas is likely to be the cause, since some buildings are more sensitive to acceleration than others, depending on their period of resonance (i.e. stiff or flexible buildings). The following sections will therefore focus mainly on velocity IMs, testing the variability observed in relation to the class of structure in particular, and assuming an insignificant effect of the tectonic context.

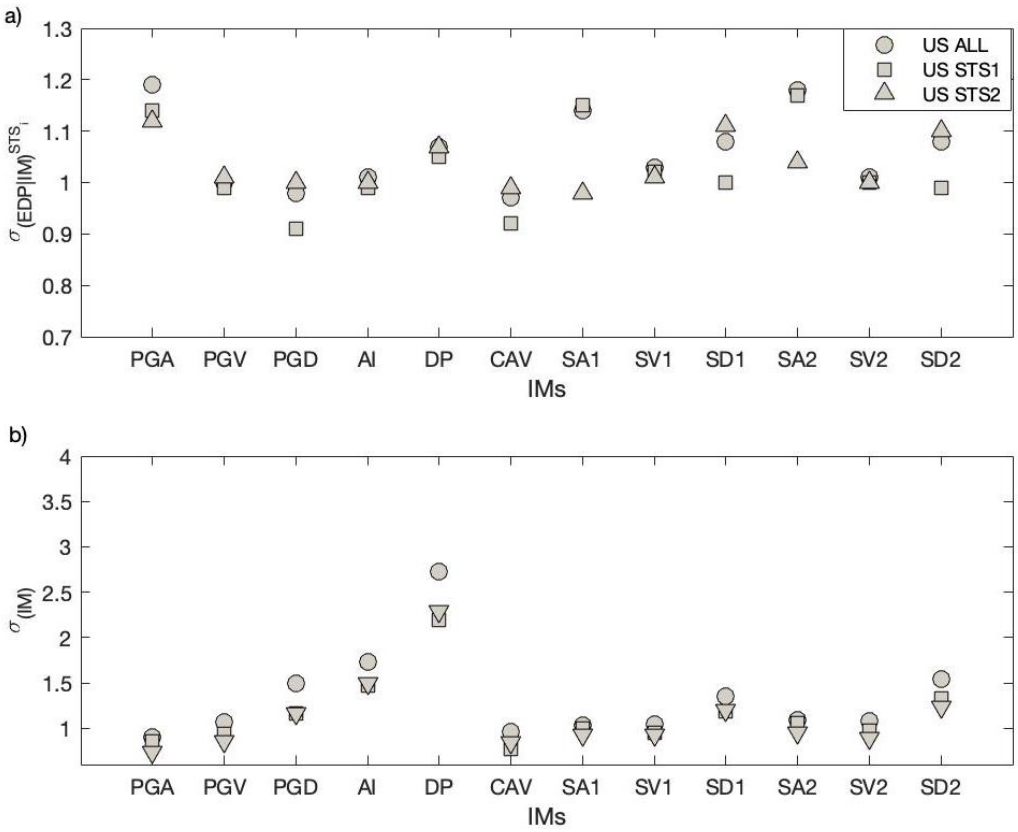

Figure 6. (a) Values of $\sigma_{EDP|IM}$ for the IMs concerned computed for US buildings by tectonic region (US STS1 and US STS2) and for all US buildings (US ALL). (b) σ_{IM} values associated with each IM.

4.3 Epistemic uncertainties related to building typology - σ_T

In this section, the variability associated with different classes of buildings is explored using the US and JPN datasets considering the description of the buildings in terms of material. Fig. 7(a) shows the variability observed for different classes of buildings in the US dataset. The trends are the same as those observed previously between the velocity IMs and the other IMs. Two typologies stand out: MA and WO. For these two typologies, the small amount of data in our dataset does not allow a more detailed analysis nor a definitive conclusion as to the effectiveness of certain IMs for EDP prediction. For the US classes (Fig. 7a), the type of structure only has a slight influence on the $\sigma_{EDP|IM}$ values for the velocity IMs (i.e. 0.94 and 0.93 for PGV, 1.01 and 1.02 for SV1, and 0.99 and 0.98 for SV2 for RC and ST, respectively, Appendix A1). On the other hand, a notable difference exists between US ST and US RC buildings in particular, the latter having a lower $\sigma_{EDP|IM}$ value for displacement IMs (i.e. 0.94 and 0.91 for PGD, 0.91 and 0.99 for SD1 for RC and ST buildings, respectively).

Significant differences between the JPN data (Fig. 7b) and the US data are observed. First of all, the velocity IMs give different $\sigma_{EDP|IM}$ values for different classes of buildings (e.g. 0.86 and 0.76 for PGV, 0.86 and 0.70 for SV1 and 0.82 and 0.50 for SV2 for JPN RC and JPN ST buildings, respectively). Fig. 7c compares the $\sigma_{EDP|IM}$ values for one specific single building (ANX building) with those of its building class conforming the epistemic uncertainties. There is a significant contribution to the specific single building $\sigma_{EDP|IM}$ values, with significantly reduced $\sigma_{EDP|IM}$ values (e.g., 0.64 to 0.50 for PGV, 0.61 to 0.48 for SV1, and 0.60 to 0.40 for SV2).

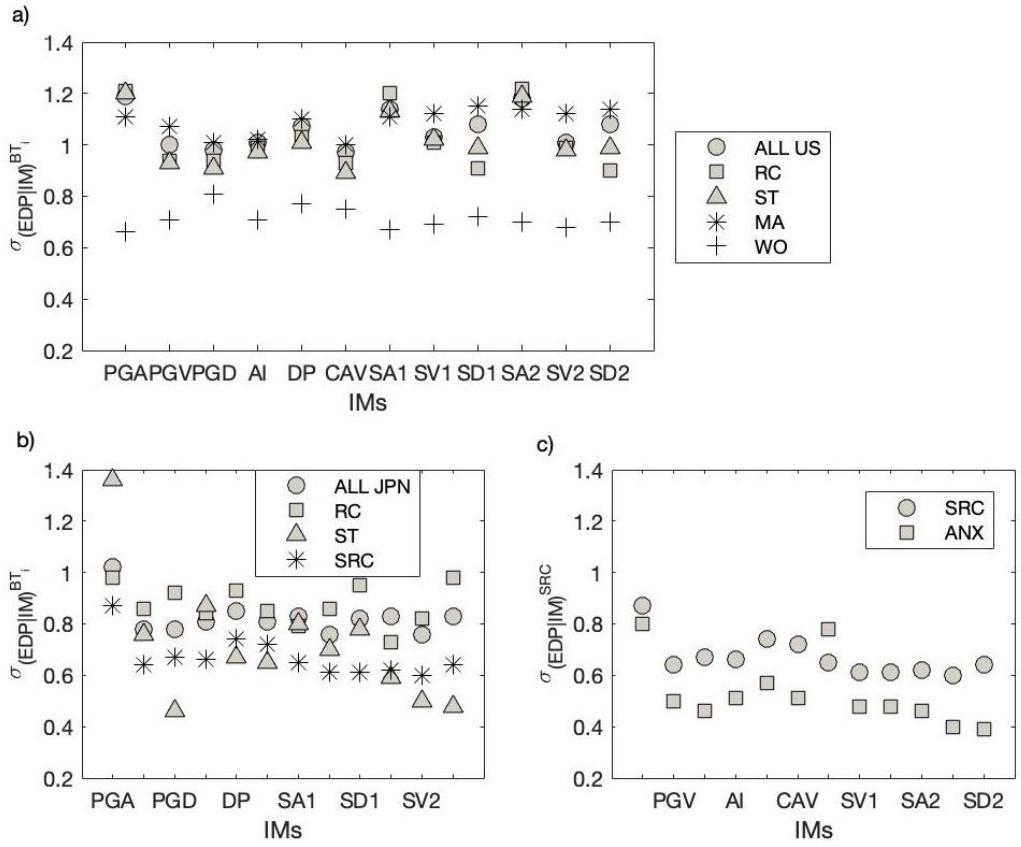

Figure 7. Variability of $\sigma_{EDP|IM}$ values as a function of the class of buildings (a) US dataset, (b) JPN dataset, (c) ANX single building dataset.

4.4 Within-building variability associated with earthquake magnitude-distance - σ_{MR}

Fig. 8a shows the effect of M/R pairs on the variability of the ANX building response. The M/R criteria are described in Fig. 3. For MR1 and MR2, the $\sigma_{EDP|IM}$ values are lower than the values of the ANX dataset, particularly for the velocity IMs (values for PGV/SV1/SV2 are 0.50/0.48/0.40 for all ANX data compared with 0.42/0.40/0.34 for MR1 and 0.41/0.41/0.37 for MR2) and for the displacement IMs (values for PGD/SD1/SD2 are 0.46/0.48/0.39 for all ANX data compared with 0.38/0.37/0.33 for MR1 and 0.35/0.42/0.29 for MR2). Thus, by taking into account the magnitude and distance the $\sigma_{EDP|IM}$ values changed significantly, regardless of the IMs considered.
Similarly, IM sufficiency is tested by considering the JPN building class dataset. For the JPN building class, Fig. 8b shows the p-value considering all the IM parameters, summarized in Tab. 7. Based on Fig. 8b, it appears difficult to conclude on the sufficiency of the IMs tested on our dataset, i.e. EDP is not conditionally independent with earthquake magnitude and distance. This result also shows that the building classes affect the IM sufficiency, for e.g. SV2 is observed to be sufficient for RC building class but not in SRC and ST building class. These results suggest that particular attention should be paid when selecting the accelerometric time histories used to perform non-linear time history analysis or PBEE assessment. Furthermore, if insufficient IMs are considered, site-specific ground motion data must be provided to avoid inaccurate estimation of the damage levels or failure rates used in PBEE if the ground motion characteristics do not match the source and site requirements (Kazantzi & Vamvatsikos, 2015).

Table 7 – p-values for the whole JPN dataset, and by JPN building class. Values in bold are greater than 0.05, i.e. the threshold for evaluating IM sufficiency.

		PGA	PGV	PGD	AI	DP	CAV	SA1	SV1	SD1	SA2	SV2	SD2
All	M	0.00	0.00	0.00	0.00	**0.47**	0.03	0.00	0.00	0.00	0.00	0.00	0.00
JPN	R	0.00	0.00	0.00	0.00	0.00	0.00	0.00	0.00	**0.13**	0.00	**0.78**	0.00

RC	M	0.00	0.00	**0.23**	0.00	**0.07**	0.00	0.00	0.00	0.00	0.00	**0.42**	0.00
	R	0.00	0.00	**0.84**	0.00	0.00	0.00	0.00	0.00	**0.05**	**0.80**	**0.06**	0.00
SRC	M	0.00	0.00	0.01	0.00	**0.21**	**0.50**	0.00	0.00	0.00	0.00	0.00	0.02
	R	0.00	0.00	0.01	0.00	0.00	0.00	0.00	0.00	0.00	0.00	0.00	**0.24**
ST	M	0.00	0.00	**0.57**	0.00	0.00	0.00	0.00	0.00	0.00	0.00	0.00	**0.41**
	R	0.00	0.00	0.03	0.00	**0.74**	0.00	0.00	0.00	**0.44**	0.00	0.00	0.00

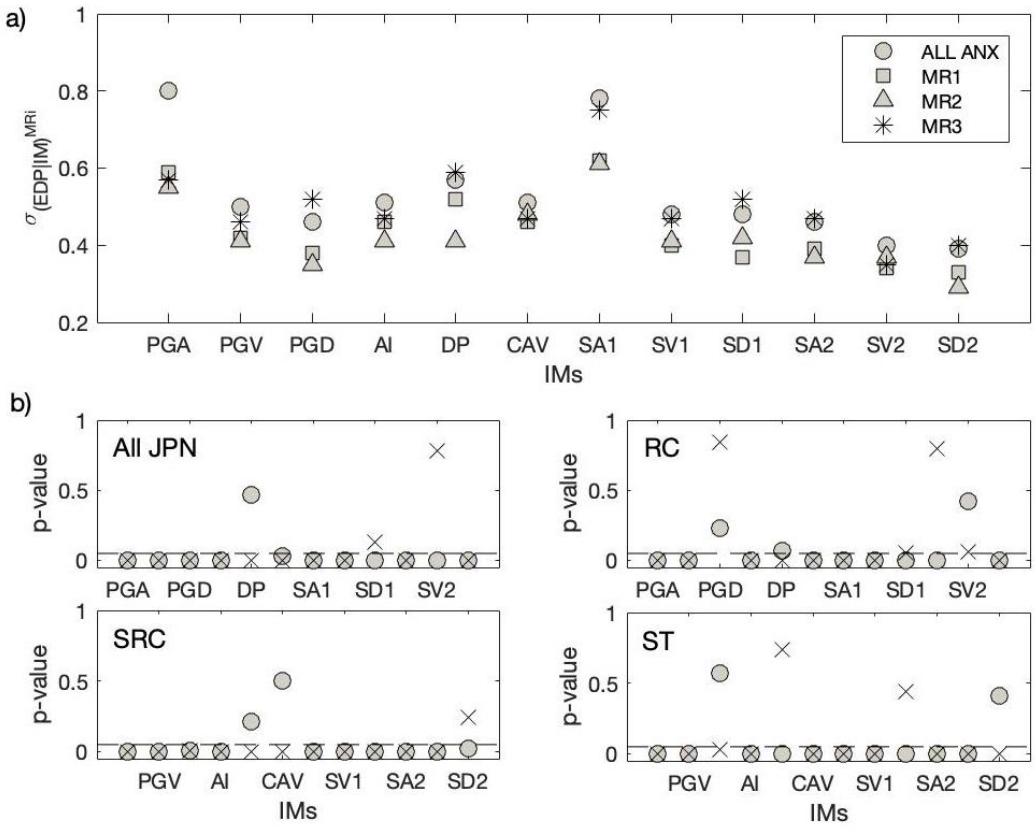

Figure 8. (a) Variability of $\sigma_{EDP|IM}$ values as a function of the IMs concerned for different magnitude and earthquake-to-building distance criteria, considering the ANX single building dataset. Magnitude/distance criteria are R = 20 ± 50% and M= 3.5 ± 0.5 for MR1; R =120 ± 60% and M= 4.5 ± 0.5 for MR2; R = 250 ± 70% and M= 5.5 ± 0.5 for MR3. (b) Sufficiency analysis with respect to magnitude (o) and distance (x) observed for the JPN building class datasets. The dashed line corresponds to a p-value of 0.05.

4.5 Within-building variability associated with aging - σ_A

Fig. 9 shows the $\sigma_{EDP|IM}$ variations as a function of the age of the ANX building. The four periods dataset corresponds to the ANX are considered here, focusing only on the M/R dataset corresponding to MR2 (i.e. the dataset with the most data). Taking into account the actual structural state of the structure lowers the $\sigma_{EDP|IM}$. For example, for PGV/SV1/SV2, the $\sigma_{EDP|IM}$ values correspond to 0.39/0.37/0.35 for the MR2-T2 ANX dataset and 0.37/0.37/0.26 for the MR2-T3 ANX dataset, compared with 0.41/0.41/0.37 for the MR2 ANX dataset as a whole. A progressive reduction of $\sigma_{EDP|IM}$ values is observed between T1 and T4, the last two periods being the most efficient (Appendix A1). It, therefore, appears that taking into account the aging or actual state of a structure in performance analysis will help to modify the associated uncertainty, $\sigma_{EDP|IM}$, ultimately changing the efficiency of IM.

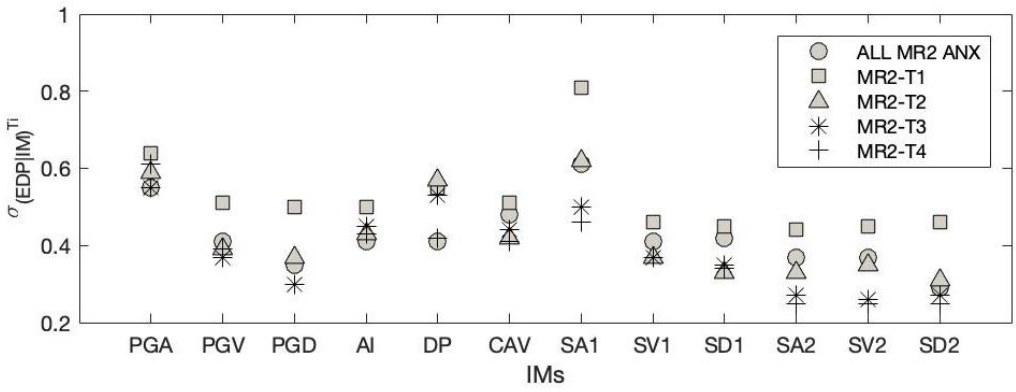

Figure 9. Variation of $\sigma_{EDP|IM}$ values as a function of the IMs for different periods, considering seismic cumulative damage in the ANX building. Magnitude/distance criteria (MR2) are R =120 ± 60% and M= 4.5 ± 0.5 and periods T1 to T4 are described in the manuscript.

4.6 Summary

Fig. 10 is a summary of the identification of the building response prediction uncertainties for the different IMs considered, based on available data and metadata. Tab. 8 summarizes the contribution of each component to the epistemic uncertainties of Eq. 9. While the regional distinction (σ_R) does not bring any significant gain (4% on average). It could be because of the fact that the Japanese dataset shares the higher portion in the whole dataset which may have impacted the value of sigma corresponding to the whole dataset. Similarly, distinction by type of construction (σ_T) and specific building (σ_B) contributes significantly (19% and 21% respectively). Concerning the IMs that make EDP conditionally independent from magnitude M and source-to-site distance (σ_{MR}), the figure shows that all the IMs are globally non-sufficient, with a reduction of $\sigma_{EDP|IM}$ values of approximately 19% for the specific case of the ANX building. When aging (σ_A), i.e. the actual health of the structure, is taken into account, the $\sigma_{EDP|IM}$ values are reduced by 8%. Spectral values considering the co-seismic shifting of the fundamental period (index 2) (SA2, SV2, and SD2) allow a reduction of the $\sigma_{EDP|IM}$ values of approximately 10%. Globally, PGV, SV1, and SV2 are observed to be the most efficient IM, i.e. they are associated with the lowest value of $\sigma_{EDP|IM}$.

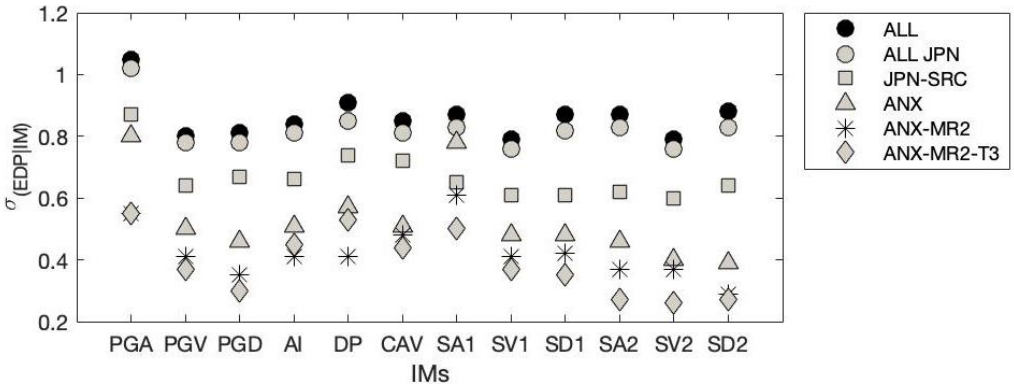

Figure 10. Summary of the variation of $\sigma_{EDP|IM}$ values as a function of the IMs concerned, considering different components of the uncertainties in prediction models.

Table 8 – Summary of the $\sigma_{EDP|IM}$ values and their reduction (in %) applied to the specific ANX building. The Avg column is the mean value of all IMs.

	PGA	PGV	PGD	AI	DP	CAV	SA1	SV1	SD1	SA2	SV2	SD2	Avg.
σ	1.05	0.80	0.81	0.84	0.91	0.85	0.87	0.79	0.87	0.87	0.79	0.88	**0.86**

σ_R	1.02	0.78	0.78	0.81	0.85	0.81	0.83	0.76	0.82	0.83	0.76	0.83	**0.82**
σ_R/σ	3 %	3 %	4 %	4 %	7 %	5 %	5 %	4 %	6 %	5 %	4 %	6 %	**4 %**
σ_T	0.87	0.64	0.67	0.66	0.74	0.72	0.65	0.61	0.61	0.62	0.60	0.64	**0.67**
σ_T/σ_R	15 %	18 %	14 %	19 %	13 %	11 %	22 %	20 %	26 %	25 %	21 %	23 %	**19 %**
σ_B	0.80	0.50	0.46	0.51	0.57	0.51	0.78	0.48	0.48	0.46	0.40	0.39	**0.53**
σ_B/σ_T	8 %	22 %	31 %	23 %	23 %	29 %	-20 %	21 %	21 %	26 %	33 %	39 %	**21 %**
σ_{MR}	0.55	0.41	0.35	0.41	0.41	0.48	0.61	0.41	0.42	0.37	0.37	0.29	**0.42**
σ_{MR}/σ_B	31 %	18 %	24 %	20 %	28 %	6 %	22 %	15 %	13 %	20 %	8 %	26 %	**19 %**
σ_A	0.55	0.37	0.30	0.45	0.53	0.44	0.50	0.37	0.35	0.27	0.26	0.27	**0.39**
σ_A/σ_{MR}	0 %	10 %	14 %	-10 %	-29 %	8 %	18 %	10 %	17 %	27 %	30 %	7 %	**8 %**
σ_A/σ	48 %	54 %	63 %	46 %	42 %	48 %	43 %	53 %	60 %	69 %	67 %	69 %	**55 %**

5. Building frequency variation and the average response spectral value as an IM

In this study, the frequency variation with respect to EDP is observed for the JPN dataset by building class. Fig. 11 summarizes the variation of the frequency ratio $fr=f_{min}/f_i$ between pre-seismic frequency (f_i) and co-seismic frequency f_{min} with respect to EDP for different JPN building classes and the whole US database, with EDP ranging from $5x10^{-6}$ to 10^{-2}. The variation of fr confirms that, regardless of building class, the frequency shift between the pre- and the co-seismic period increases with EDP, which means large frequency drops occur for the strongest earthquakes. A significant variation of f_r is observed even at the lower end of the EDP range from 0.9 to 0.65 (below the slight damage threshold=0.0025). For EDP values between 10^{-5} and 10^{-3}, a relatively similar trend is observed regardless of building class, with fr values decreasing from 0.78 to 0.65. The non-linear variation of the building frequency for EDP < 10^{-3} may be linked with the slow dynamics phenomenon and soil-structure interaction (Astorga et al. 2018). There are no stronger earthquakes, this result suggests the need to collect a large amount of earthquake data in buildings in order to refine our performance prediction models.

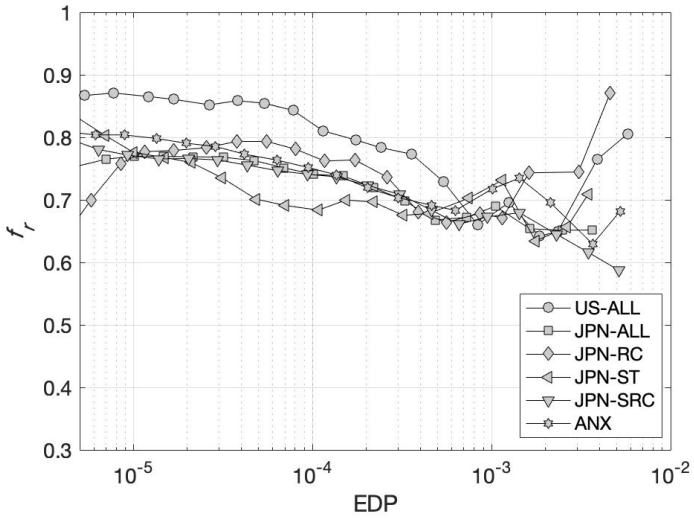

Figure 11 – Variation of the frequency ratio ($f_r=f_{min}/f_i$) for different datasets.

6. Conclusions

Experimental data is very useful in helping us to understand the complex physical processes that occurs in civil engineering structures to be able to integrate them into our

models to reduce the epistemic uncertainty of these complex process. Earthquake data collected from buildings under long-term monitoring in Japan, the US, and Romania were used to attempt to identify the components of the building response prediction uncertainties. Region-to-region, building-to-building, and within-building uncertainties associated with earthquake magnitude-distance and aging were explored.

Compared with the conventional IMs based on peak values or conventional spectral value (SA1, SV1 or SD1), the ground motion intensity measure, denoted SA2, SV2, and SD2, which considers inelastic period lengthening, was found to be the most efficient IM for estimating EDP, taken as structural drift herein. In terms of sufficiency, generally speaking, it appears that no IMs are sufficient due to a significant conditional dependence of EDP on R (i.e. earthquake source-to-building distance) and M (i.e. magnitude). Some exceptions are pointed out in Fig. 8 for specific building classes and IMs. In fact, depending on the type of building and, in particular, its period, displacement, and acceleration IMs might be more efficient or sufficient; this could be confirmed with additional data and a specific analysis of the building characteristics, which is not considered by this study. Nevertheless, all our results indicate that velocity IMs (PGV, SV1, SV2) are those that provide the lowest variability for predicting EDP given IM.

Based on the ANX building results, the components that make the largest contribution to overall uncertainties are building class and specific building associated with the M/R condition (Fig. 10, Tab. 8). When analyzing specific buildings using long-term monitoring data, the real structural state also appears to make a significant contribution to the uncertainties, reflecting the real co-seismic demand in EDP prediction. The underlying key issue is related to the variation of frequency, which is strongly dependent on EDP. Note that regardless of building class, this frequency variation follows the same trend for all the drift values in our dataset. In general, the seismic analysis and PBEE is carried out by considering the height and material. Limited studies have been carried out by considering the real structural state of the structures. We found out that taking into account the actual structural state could reduce the sigma by 8% in average and 30% for the most efficient IMs (Tab. 8). This result highlights the importance of instrumentation and continuous monitoring of the health of the structures in order to have a reliable assessment of the potential loss due to earthquakes. In addition, having more information on the earthquakes and descriptions of the building characteristics would help to improve the prediction of structural response for analyzing seismic vulnerability or loss assessment. Although the amount of data contained in our dataset provides relevant results, the paucity of data concerning specific classes of buildings or components of uncertainties limits the strength of the conclusions that can be drawn. To resolve outstanding issues, we must continue our international collaborative efforts and motivate building owners to share their data, which would increase their interest in this type of study. In particular, having more specific data would enable verification of the aforementioned conclusions.

Moreover, building response prediction models can be developed considering several parameters related to earthquakes and buildings, such as ground motion IM, magnitude, distance, building typology, height, structural properties, etc. (FEMA, 1999; Hancock et al., 2008; Perrault & Guéguen, 2015). In conclusion to this study, an empirical building damage prediction model is proposed (Tab. 9) based on the entire dataset (US, Japan, and Romania) according to building class and considering the most efficient IMs (SV2 and PGV) using the functional form given in Eq. 9:

$$log(\mathrm{EDP}) = \mathrm{a} + \mathrm{b}.\log(\mathrm{IM}) + \varepsilon$$

Table 9- Empirical building damage prediction model according to building class.

IM	Parameter	BT-ALL	BT-RC	BT-SRC	BT-ST	BT-MA	BT-WO
SV2	a	-10.22	-10.65	-10.00	-9.81	-9.17	-9.26
	b	0.87	0.83	0.89	1.08	0.55	0.58
	σ	0.79	0.84	0.60	0.60	1.10	0.68
PGV	a	-9.41	-9.78	-9.21	-9.17	-8.80	-9.02
	b	0.94	0.86	0.95	1.16	0.60	0.55
	σ	0.80	0.87	0.64	0.80	1.07	0.71

Several seismic risk assessment frameworks consider building heights as one of the criteria in building classification. Further investigations on the variation of sigma could be carried out by grouping the buildings according to the height of the buildings. Fig. 11 shows a significant variation of the building frequency as a function of EDP, additional investigation on the efficiency and sufficiency of IMs over different EDP ranges could be carried to explore the contribution of change in the real structural state of structures. Studies have shown that the soil-structure interaction plays a significant role in the structural response, investigation on the variation of sigma due to the soil-structure interaction system could be interesting. In addition, the early-warning parameters available in the database could be used to investigate the relationship between early warning parameters and the structural response in order to develop building response prediction models for onsite early warning systems.

Acknowledgments

This work is funded by the URBASIS-EU project (H2020-MSCA-ITN-2018, grant number 813137). Japanese data were obtained from the BRI Strong Motion Observation (http:// smo.kenken.go.jp/). US data were provided by the Center for Engineering Strong Motion Data (CESMD, https://strongmotioncenter.org/). Romanian data were obtained from the National Center for Seismic Risk Reduction (NCSRR, http://cnrrs.utcb.ro/cnrrs_en/). P.G. would like to thank LabEx OSUG@2020 (Investissements d'avenir-ANR10LABX56). Part of this work was supported by the Seismology and Earthquake Engineering Research Infrastructure Alliance for Europe (SERA), a project funded by the EU Horizon 2020 program under Grant Agreement Number 730900.

References

Araya, R., & Saragoni, G. R. (1984). Earthquake accelerogram destructiveness potential factor. *Paper Presented at the Proc. 8th World Conference on Earthquake Engineering*, 7.

Arias, A. (1970). *MEASURE OF EARTHQUAKE INTENSITY*.

Astorga, A., Guéguen, P., Ghimire, S., & Kashima, T. (2020). NDE1.0: a new database of earthquake data recordings from buildings for engineering applications. *Bulletin of Earthquake Engineering*, *18*(4), 1321–1344. https://doi.org/10.1007/s10518-019-00746-6

Astorga, A., Guéguen, P., & Kashima, T. (2018). Nonlinear elasticity observed in buildings during a long sequence of earthquakes. *Bulletin of the Seismological Society of America*, *108*(3), 1185–1198. https://doi.org/10.1785/0120170289

Astorga, A. L., Guéguen, P., Rivière, J., Kashima, T., & Johnson, P. A. (2019). Recovery of the resonance frequency of buildings following strong seismic deformation as a proxy for structural health. *Structural Health Monitoring*, *18*(5–6), 1966–1981. https://doi.org/10.1177/1475921718820770

Baker, J. W., & Cornell, C. A. (2008a). Uncertainty propagation in probabilistic seismic loss estimation. *Structural Safety*, *30*(3), 236–252. https://doi.org/10.1016/j.strusafe.2006.11.003

Baker, J. W., & Cornell, C. A. (2008b). Vector-valued intensity measures incorporating spectral shape for prediction of structural response. In *Journal of Earthquake Engineering* (Vol. 12, Issue 4). https://doi.org/10.1080/13632460701673076

Benjamin, J. R., & Cornell, C. A. (1970). *Solutions Manual to Accompany Probability, Statistics and Decision for Civil Engineer*. McGraw-Hill.

Bianchini, M., Diotallevi, P. P., & Baker, J. W. (2009). *Prediction of Inelastic Structural Response Using an Average of Spectral Accelerations*. 8. http://www.sc.kutc.kansai-u.ac.jp/icossar2009/index.html

Buratti, N. (2012). A comparison of the performances of various ground–motion intensity measures. *In 15th World Conference on Earthquake Engineering, Lisbon, Portugal*, 77.

Eads, L., Miranda, E., & Lignos, D. . (2015). Average spectral acceleration as an intensity measure for collapse risk assessment. *Earthquake Engineering & Structural Dynamics*, *44*(12), 2057–2073. https://doi.org/10.1002/eqe

Ebrahimian, H., Jalayer, F., Lucchini, A., Mollaioli, F., & Manfredi, G. (2015). Preliminary ranking of alternative scalar and vector intensity measures of

ground shaking. *Bulletin of Earthquake Engineering*, *13*(10), 2805–2840. https://doi.org/10.1007/s10518-015-9755-9
EPRI. (1988). *A Criterion for Determining Expedience of the Operating Basis Earthquake*.
FEMA, F. (1999). *Case Studies-An Assessment of the NEHRP Guidelines for the Seismic Rehabilitation of Buildings.*
Guéguen, P., Johnson, P., & Roux, P. (2016). Nonlinear dynamics induced in a structure by seismic and environmental loading. *The Journal of the Acoustical Society of America*, *140*(1), 582–590. https://doi.org/10.1121/1.4958990
Hancock, J., Bommer, J. J., & Stafford, P. J. (2008). Numbers of scaled and matched accelerograms required for inelastic dynamic analyses. *Earthquake Engineering & Structural Dynamics*, *14*(37), 1585–1607.
Iervolino, I. (2017). Assessing uncertainty in estimation of seismic response for PBEE. *Earthquake Engineering & Structural Dynamics*, *46*(10), 171101723. https://doi.org/10.1002/eqe
Jayaram, N., Lin, T., & Baker, J. W. (2011). A Computationally efficient ground-motion selection algorithm for matching a target response spectrum mean and variance. *Earthquake Spectra*, *27*(3), 797–815. https://doi.org/10.1193/1.3608002
Kashima, T. (2004). Dynamic Behavior of an Eight-Storey SRC Building Examined from Strong Motion Records. *Paper Presented at the 13th World Conference on Earthquake Engineering.*
Kashima, T. (2014). Dynamic behaviour of SRC buildings damaged by the 2011 great east japan earthquake based on strong motion records. *In Second European Conference on Earthquake Engineering and Seismology*.
Kazantzi, A. K., & Vamvatsikos, D. (2015). Intensity measure selection for vulnerability studies of building classes. *Earthquake Engineering and Structural Dynamics*, *44*(15), 2677–2694. https://doi.org/10.1002/eqe.2603
Luco, N. (2002). Probabilistic seismic demand analysis, SMRF connection fractures, and near-source effects. *Department of Civil and Environmental\rEngineering*, *June*, 260 pp. http://search.proquest.com/docview/305541530?accountid=13014
Luco, N., & Cornell, C. A. (2007). Structure-specific scalar intensity measures for near-source and ordinary earthquake ground motions. *Earthquake Spectra*, *23*(2), 357–392.
Luco, N., Manuel, L., Baldava, S., & Bazzurro, P. (2005). Correlation of damage of steel moment-resisting frames to a vector-valued set of ground motion parameters. *Proceedings of the 9th International Conference on Structural Safety and Reliability (ICOSSAR05)*, 2719–2726.
Mollaioli, F., Silvia, B., Luis, D., & Rodolfo, S. (2011). Correlations between energy and displacement demands for performance-based seismic engineering. *Pure and Applied Geophysics*, *168*(1–2), 237–259. https://doi.org/10.1007/s00024-010-0118-9
Perrault, M., & Guéguen, P. (2015). Correlation between ground motion and building response using California earthquake records. *Earthquake Spectra*, *31*(4), 2027–2046. https://doi.org/10.1193/062413EQS168M
Porter, K. (2003). An overview of PEER's performance-based earthquake engineering methodology. *In : Proceedings of Ninth International Conference on Applications of Statistics and Probability in Civil Engineering (ICASP9), San Francisco (US)*.
Todorovska, M. I., & Trifunac, M. D. (2007). Earthquake damage detection in the Imperial County Services Building I: The data and time-frequency analysis. *Soil Dynamics and Earthquake Engineering*, *27*(6), 564–576. https://doi.org/10.1016/j.soildyn.2006.10.005
Trifunac, M. D., & Brady, A. G. (1975). A study on the duration of strong earthquake ground motion. *Bulletin of the Seismological Society of America*, *3*(65), 581–626.
Trifunac, M. D., Todorovska, M. I., Manić, M. I., & Bulajić, B. Đ. (2010). Variability of the fixed-base and soil–structure system frequencies of a building—The case of Borik-2 building. *Structural Control and Health Monitoring: The Official Journal of the International Association for Structural Control and Monitoring and of the European Association for the Control of Structures*, *2*(17), 120–15. https://doi.org/10.1002/stc
Vamvatsikos, D., & Cornell, C. A. (2005). Developing efficient scalar and vector intensity measures for IDA capacity estimation by incorporating elastic spectral shape information. *Earthquake Engineering and Structural Dynamics*, *34*(13), 1573–1600. https://doi.org/10.1002/eqe.496
Zhou, Y., & Xie, L. L. (1984). A new definition of strong ground

motion duration. *Earthquake Engineering and Engineering Vibration*, *4*(2).

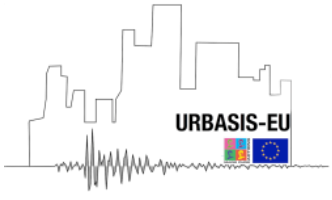

Appendix

Table A1. σ_{IM}, σ_{EDP}, and $\sigma_{EDP|IM}$ values considering different sub datasets discussed in the manuscript

			PGA	PGV	PGD	AI	DP	CAV	SA1	SV1	SD1	SA2	SV2	SD2
US+JPN +RO	ALL	IM	1.15	1.33	1.63	2.29	3.35	1.21	1.53	1.31	1.43	1.63	1.44	1.61
		EDP	1.48	1.48	1.48	1.48	1.48	1.48	1.48	1.48	1.48	1.48	1.48	1.48
		EDP|IM	1.05	0.80	0.81	0.84	0.91	0.85	0.87	0.79	0.87	0.87	0.79	0.88
US data	ALL	IM	0.90	1.07	1.49	1.73	2.73	0.96	1.03	1.04	1.35	1.09	1.08	1.54
		EDP	1.32	1.32	1.32	1.32	1.32	1.32	1.32	1.32	1.32	1.32	1.32	1.32
		EDP|IM	1.19	1.00	0.98	1.01	1.07	0.97	1.14	1.03	1.08	1.18	1.01	1.08
	STS1	IM	0.86	0.94	1.15	1.48	2.20	0.77	1.00	1.06	1.20	1.03	1.08	1.31
		EDP	1.24	1.24	1.24	1.24	1.24	1.24	1.24	1.24	1.24	1.24	1.24	1.24
		EDP|IM	1.14	1.00	0.93	1.00	1.07	0.93	1.15	1.03	1.03	1.15	1.01	1.03
	STS2	IM	0.74	0.85	1.15	1.49	2.29	0.84	0.92	0.95	1.20	0.95	0.92	1.29
		EDP	1.20	1.20	1.20	1.20	1.20	1.20	1.20	1.20	1.20	1.20	1.20	1.20
		EDP|IM	1.12	1.01	0.99	1.00	1.06	0.98	0.97	1.01	1.10	1.04	1.01	1.10
	RC	IM	0.84	0.98	1.47	1.58	2.63	0.91	1.03	1.03	1.25	1.07	1.04	1.31
		EDP	1.32	1.32	1.32	1.32	1.32	1.32	1.32	1.32	1.32	1.32	1.32	1.32
		EDP|IM	1.21	0.94	0.94	0.99	1.03	0.93	1.20	1.01	0.91	1.22	0.99	0.90
	ST	IM	0.84	1.01	1.46	1.55	2.78	0.87	0.91	1.02	1.32	0.99	1.08	1.64
		EDP	1.28	1.28	1.28	1.28	1.28	1.28	1.28	1.29	1.28	1.28	1.29	1.28
		EDP|IM	1.20	0.93	0.91	0.97	1.01	0.89	1.13	1.02	0.99	1.19	0.98	0.99
	MA	IM	0.91	1.08	1.43	1.83	2.35	1.02	0.94	1.27	1.71	1.00	1.18	1.46
		EDP	1.23	1.23	1.23	1.23	1.23	1.23	1.23	1.21	1.21	1.23	1.23	1.23
		EDP|IM	1.11	1.07	1.01	1.02	1.10	1.00	1.11	1.12	1.15	1.14	1.12	1.14
	WO	IM	1.02	1.36	1.83	2.20	3.21	1.21	1.07	1.32	1.60	1.06	1.32	1.65
		EDP	1.02	1.02	1.02	1.02	1.02	1.02	1.02	1.02	1.02	1.02	1.02	1.02
		EDP|IM	0.66	0.71	0.81	0.71	0.77	0.75	0.67	0.69	0.72	0.70	0.68	0.70
Japanese	ALL	IM	1.11	1.31	1.61	2.26	3.34	1.22	1.50	1.30	1.42	1.61	1.43	1.61
		EDP	1.44	1.44	1.44	1.44	1.44	1.44	1.44	1.44	1.44	1.44	1.44	1.44
		EDP|IM	1.02	0.78	0.78	0.81	0.85	0.81	0.83	0.76	0.82	0.83	0.76	0.83
	RC	IM	0.98	1.13	1.50	2.02	2.98	1.12	1.25	1.09	1.22	1.37	1.20	1.35
		EDP	1.28	1.28	1.28	1.28	1.28	1.28	1.28	1.28	1.28	1.28	1.28	1.28
		EDP|IM	0.98	0.86	0.92	0.84	0.93	0.85	0.79	0.86	0.95	0.73	0.82	0.98
	SRC	IM	1.14	1.40	1.66	2.36	3.53	1.24	1.48	1.37	1.46	1.56	1.52	1.68
		EDP	1.48	1.48	1.48	1.48	1.48	1.48	1.48	1.48	1.48	1.48	1.48	1.48
		EDP|IM	0.87	0.64	0.67	0.66	0.74	0.72	0.65	0.61	0.61	0.62	0.60	0.64
	ST	IM	1.11	1.24	1.61	2.18	3.24	1.21	1.72	1.37	1.56	1.65	1.43	1.70
		EDP	1.67	1.67	1.67	1.67	1.67	1.67	1.67	1.67	1.67	1.67	1.67	1.67
		EDP|IM	1.36	0.76	0.46	0.87	0.67	0.65	0.80	0.70	0.78	0.59	0.50	0.48
ANX building	ALL	IM	1.00	1.27	1.51	2.12	3.25	1.13	1.54	1.31	1.42	1.44	1.41	1.59
		EDP	1.42	1.42	1.42	1.42	1.42	1.42	1.42	1.42	1.42	1.42	1.42	1.42
		EDP|IM	0.80	0.50	0.46	0.51	0.57	0.51	0.78	0.48	0.48	0.46	0.40	0.39
	STS	IM	1.01	1.28	1.50	2.13	3.25	1.13	1.55	1.32	1.43	1.45	1.42	1.60
		EDP	1.43	1.43	1.43	1.43	1.43	1.43	1.43	1.43	1.43	1.43	1.43	1.43
		EDP|IM	0.80	0.50	0.45	0.50	0.56	0.50	0.78	0.48	0.47	0.45	0.39	0.39
	MR1	IM	0.69	0.80	0.90	1.30	2.10	0.65	1.06	0.85	0.91	0.89	0.88	0.97
		EDP	0.86	0.86	0.86	0.86	0.86	0.86	0.86	0.86	0.86	0.86	0.86	0.86
		EDP|IM	0.59	0.42	0.38	0.46	0.52	0.46	0.62	0.40	0.37	0.39	0.34	0.33
	MR2	IM	0.71	0.75	0.78	1.16	1.82	0.57	1.21	0.79	0.89	0.89	0.79	0.86

	EDP	0.71	0.71	0.71	0.71	0.71	0.71	0.71	0.71	0.71	0.71	0.71	0.71
	EDP|IM	0.55	0.41	0.35	0.41	0.41	0.48	0.61	0.41	0.42	0.37	0.37	0.29
MR3	IM	0.79	0.86	0.96	1.47	2.17	0.73	1.10	0.85	0.93	0.88	0.92	1.03
	EDP	1.02	1.02	1.02	1.02	1.02	1.02	1.02	1.02	1.02	1.02	1.02	1.02
	EDP|IM	0.57	0.46	0.52	0.47	0.59	0.47	0.75	0.47	0.52	0.47	0.35	0.40
T1-MR2	IM	0.83	0.95	1.02	1.58	2.19	0.81	1.18	0.92	0.99	0.98	0.98	1.05
	EDP	0.94	0.94	0.94	0.94	0.94	0.94	0.94	0.94	0.94	0.94	0.94	0.94
	EDP|IM	0.64	0.51	0.50	0.50	0.55	0.51	0.81	0.46	0.45	0.44	0.45	0.46
T2-MR2	IM	0.66	0.77	0.89	1.24	1.93	0.61	1.17	0.86	0.94	0.86	0.84	0.90
	EDP	0.85	0.85	0.85	0.85	0.85	0.85	0.85	0.85	0.85	0.85	0.85	0.85
	EDP|IM	0.59	0.39	0.37	0.43	0.57	0.42	0.62	0.37	0.33	0.33	0.35	0.31
T3-MR2	IM	0.60	0.71	0.80	1.14	1.98	0.57	0.91	0.78	0.82	0.79	0.80	0.90
	EDP	0.80	0.80	0.80	0.80	0.80	0.80	0.80	0.80	0.80	0.80	0.80	0.80
	EDP|IM	0.55	0.37	0.30	0.45	0.53	0.44	0.50	0.37	0.35	0.27	0.26	0.27
T4-MR2	IM	0.63	0.75	0.90	1.22	2.13	0.61	0.98	0.83	0.87	0.91	0.89	1.01
	EDP	0.80	0.80	0.80	0.80	0.80	0.80	0.80	0.80	0.80	0.80	0.80	0.80
	EDP|IM	0.61	0.39	0.30	0.43	0.42	0.41	0.46	0.37	0.34	0.25	0.25	0.25